

# Allowed and forbidden Raman scattering mechanisms for detection of coherent LO phonon and plasmon-coupled modes in GaAs

Kunie Ishioka\*

*Nano Characterization Unit, National Institute for Materials Science, Tsukuba, 305-0047 Japan*

Amlan Kumar Basak and Hrvoje Petek

*Department of Physics and Astronomy, University of Pittsburgh, Pittsburgh, Pennsylvania 15260, USA*

(Received 6 September 2011; published 1 December 2011)

Detection mechanisms of coherent phonons in variously doped GaAs are investigated by transient reflectivity method with photoexcitation near the  $E_0$  gap and probe near either the  $E_0$  or  $E_1$  gaps. By varying the probe light polarization angle, the coherent amplitudes of both the LO phonon and the LO phonon-plasmon coupled (LOPC) modes show evidence for an interference between their anisotropic and isotropic dielectric response components. We attribute the anisotropic and isotropic components to the reflectivity modulation by lattice and electronic polarizations via dipole-allowed and dipole-forbidden Raman scattering processes. The forbidden processes are resonantly enhanced at the  $E_0$  and  $E_1$  critical points due to the relaxation of momentum conservation and the strong built-in electric field near the surface. The relative contribution of the anisotropic and isotropic components depends on the modes (LO or LOPC) as well as the probe wavelength ( $E_0$  or  $E_1$ ), because of the different Raman scattering mechanisms involved. Reflectivity measurements with the near-ultraviolet light, which is used to probe the  $E_1$  gap, also enable highly surface sensitive detection of ultrafast LO phonon-plasmon dynamics, which is strongly depth dependent in the depletion layer of  $n$ -doped GaAs.

DOI: [10.1103/PhysRevB.84.235202](https://doi.org/10.1103/PhysRevB.84.235202)

PACS number(s): 78.47.jg, 63.20.kd, 78.30.Fs

## I. INTRODUCTION

Illumination of crystalline surfaces by ultrashort light pulses can impulsively excite coherent phonons of the optical branch. The coherent optical phonons have been observed as a periodic modulation in the THz frequency range, most conveniently by linear and nonlinear optical techniques.<sup>1-3</sup> The generation mechanisms of the coherent phonons have been studied extensively in a variety of crystals and attributed, depending on the nature of the electron-phonon interaction, to impulsive stimulated Raman scattering (ISRS),<sup>4,5</sup> displacive excitation of coherent phonons (DECP),<sup>6</sup> and transient depletion field screening (TDFS).<sup>7-9</sup> The time evolution of coherent phonons is in general determined by the phonon anharmonicity (phonon-phonon scattering)<sup>10</sup> and scattering by defects.<sup>11,12</sup> Electron-phonon scattering can also contribute to the dephasing of the coherent phonons in low-dimensional crystals<sup>13</sup> or in the presence of highly nonequilibrium carrier distributions.<sup>14</sup> Real-time observation of coherent phonons can thus probe the time-dependent electron-phonon interaction.<sup>13</sup>

Linear optical methods such as reflection offer conventional but sensitive means to monitor coherent phonon dynamics in both opaque and transparent crystalline solids. While the behavior of the dielectric constant under laser-induced phase transition has been extensively studied,<sup>15</sup> the mechanism of the reflectivity modulation by the small nuclear motion in the vicinity of the equilibrium remains largely unexplored in spite of its extensive application. Among the few experimental studies Kurz and coworkers measured the transient reflectivity response of GaAs and Ge for a few probe polarization angles.<sup>7,16,17</sup> On one hand, they found the reflectivity modulation amplitude due to the coherent LO phonon of undoped GaAs to be probe-polarization-angle dependent, which they attributed to the linear electro-optic (LEO) effect.<sup>7</sup> By contrast, for heavily  $n$ -doped GaAs, in

which the LO phonon couples with doped carriers to form LO phonon-plasmon coupled (LOPC) mode, the amplitude of the coherent LOPC mode was nearly independent of the probe polarization.<sup>16</sup> The observation was interpreted in terms of the nonlinear electro-optic (NEO), i.e., Franz-Keldysh effect. The isotropic amplitude due to the NEO effect was found to be much larger than the anisotropic amplitude due to the LEO effect for photon energies near the  $E_0$  critical point (1.42 eV at room temperature), but decreased rapidly as the photon energy was tuned away from the resonance. On the other hand, they found the amplitude of the coherent optical phonons of Ge, in which the EO effect can be neglected, to show a similar probe angle dependence to that of undoped GaAs, and attributed it to the anisotropic band-gap modulation.<sup>17,18</sup> Though these studies demonstrated a strong dependence of the LO and LOPC mode signals on the probe polarization angle, the underlying mechanisms have hardly been explored. For better understanding of the detection mechanism, a more systematic investigation of the probe polarization dependence at different critical points is required.

In the present study, we investigate the detection mechanisms of the coherent LO phonon and the LOPC modes of differently doped GaAs through the dependence of their coherent amplitudes in transient reflectivity measurements on the polarization angle  $\theta$  of the probe light with respect to the crystalline axes. We use pump pulses at 1.55 eV to excite electron-hole pairs near the fundamental gap ( $E_0$  critical point) of GaAs, and probe pulses at either 1.55 or 3.1 eV to monitor the coherent phonon-plasmon dynamics in the bulk and surface regions. We observe the interference between anisotropic and isotropic coherent amplitudes with respect to  $\theta$ , which we attribute to the reflectivity modulation via dipole-allowed and dipole-forbidden Raman scattering processes, respectively. This analysis of the different signal amplitudes

and anisotropies leads to an improved understanding of different microscopic processes operative in the detection of the LO and LOPC modes at different depths within GaAs samples.

## II. THEORETICAL BACKGROUND

### A. Generation and detection of coherent phonons

Coherent optical phonons can be described as a macroscopic classical oscillation of the crystalline lattice in which a small nuclear displacement  $Q$  within a unit cell follows the equation of motion for a driven, damped oscillator:<sup>1,2</sup>

$$\mu \left[ \frac{\partial^2 Q(t)}{\partial t^2} + 2\Gamma \frac{\partial Q(t)}{\partial t} + \Omega^2 Q(t) \right] = F(t), \quad (1)$$

with the reduced mass  $\mu$ , the phonon damping  $\Gamma$ , and the frequency  $\Omega$ . Solving the equation of motion gives the trajectory of a damped harmonic oscillator,

$$Q(t) = Q_0 \exp(-\Gamma t) \sin(2\pi \Omega t + \psi). \quad (2)$$

For the LO phonon of GaAs(001) surface irradiated with a laser pulse at normal incidence, the driving force  $F(t)$  can be described by

$$F_j(t) = R_{jkl} E_k E_l - \frac{e^*}{\varepsilon_\infty \varepsilon_0} \int_{-\infty}^t dt' J_j(t'), \quad (3)$$

where  $e^*$  is the effective lattice charge, and  $E_k$  and  $E_l$  are the pump-field components. The indices  $j$ ,  $k$ , and  $l$  denote the Cartesian coordinates, where  $j$  is the  $z = [001]$  direction of the LO phonon displacement normal to the surface and  $k$  and  $l$  denote the  $x = [100]$  and  $y = [010]$  directions.

The second term in Eq. (3) describes the ultrafast drift-diffusion current in the surface normal direction  $j$  in the presence of surface built-in field within the depletion or accumulation layer of a doped semiconductor. This current can launch coherent phonons polarized along the  $j$  direction via ultrafast screening of the built-in field (TDFS mechanism).<sup>7-9</sup> The excitation via TDFS requires photoexcitation of carriers at sufficient density for screening of the field, but does not depend explicitly on the direction of the pump electric field for a zinc-blende crystal.<sup>8</sup>

The first term in Eq. (3) represents ISRS in which a broadband femtosecond optical pulse offers multiple combinations of two-photon difference frequencies required for the stimulated Raman process ( $\hbar\omega_1 - \hbar\omega_2 = \hbar\Omega$ ).<sup>4</sup> Nonlinear susceptibility of the second order (EO effect) can be included in the Raman term, while that of the third order is negligible for a zinc-blende crystal in the present geometry.<sup>8</sup> The ISRS force depends on the direction of the applied electric field through the Raman tensor  $R_{jkl} = (\partial\chi/\partial Q)_{jkl}$ . For the LO phonon of GaAs excited in the geometry described above, the dipole-allowed Raman tensor is given by

$$\overset{\leftrightarrow}{R}_{\text{allowed}} = \begin{pmatrix} 0 & a & 0 \\ a & 0 & 0 \\ 0 & 0 & 0 \end{pmatrix}, \quad (4)$$

where  $a$  is the Raman polarizability. As the basis function corresponding to this tensor,  $z(x^2 - y^2)$ ,<sup>19</sup> varies as  $\cos(2\phi)$  with polar angle  $\phi$  within the  $xy$  plane, so should coherent LO

phonon amplitude generated by dipole-allowed ISRS when the pump polarization angle  $\phi$  is rotated.<sup>20</sup> For the dipole-forbidden Raman scattering near the  $E_0$  and  $E_1$  critical points, the tensor is given by

$$\overset{\leftrightarrow}{R}_{\text{forbidden}} = \begin{pmatrix} b & 0 & 0 \\ 0 & b & 0 \\ 0 & 0 & b \end{pmatrix}, \quad (5)$$

with  $b$  being the forbidden Raman polarizability. The amplitude of the coherent phonon generated by the dipole-forbidden ISRS should be independent of  $\phi$ ,<sup>20</sup> as the basis function for its tensor is a constant.<sup>19</sup>

In transient reflectivity measurements, a nuclear displacement  $Q$  associated with the LO phonon oscillation induces a change in reflectivity  $R$  through the refractive index  $n$  and the susceptibility  $\chi$ . In a first-order approximation, the change  $\Delta R$  is given by<sup>1,2,16</sup>

$$\Delta R = \frac{\partial R}{\partial n} \Delta n \simeq \frac{\partial R}{\partial \chi} \frac{\partial \chi}{\partial Q} \Delta Q. \quad (6)$$

As  $\partial\chi/\partial Q$  is the first-order Raman tensor, Eq. (6) implies that only Raman-active phonons can be observed, provided that the detection geometry (scattering  $k$  vector) and optical polarization satisfy the Raman selection rules.<sup>1,2</sup>

### B. LOPC modes in polar compound semiconductors

In polar semiconductors, LO phonons couple with the collective charge-density oscillations to form LOPC modes.<sup>21</sup> The frequencies of the LOPC modes are obtained by solving the equation for the frequency-dependent dielectric response of the lattice and electrons:<sup>22-24</sup>

$$\varepsilon(\omega) = \varepsilon_\infty \left[ 1 + \frac{\Omega_{\text{LO}}^2 - \Omega_{\text{TO}}^2}{\Omega_{\text{TO}}^2 - i\Gamma\omega - \omega^2} - \frac{\omega_p^2}{\omega^2 + i\gamma\omega} \right] = 0, \quad (7)$$

where  $\varepsilon_\infty$  is the high-frequency dielectric constant,  $\gamma$  and  $\Gamma$  are plasmon and phonon damping rates, and  $\Omega_{\text{LO}}$  and  $\Omega_{\text{TO}}$  are the LO and TO phonon frequencies. The plasma frequency,

$$\omega_p = \sqrt{\frac{ne^2}{m^* \varepsilon_0 \varepsilon_\infty}}, \quad (8)$$

depends on the carrier density and effective mass,  $n$  and  $m^*$ , and the vacuum dielectric constant,  $\varepsilon_0$ .

The plasma damping rate and the carrier mass depend significantly on the carrier type; the LOPC mode properties associated with electrons and holes are therefore substantially different. For  $n$ -doped GaAs, the frequencies of the LOPC mode coupled with electron plasma is reproduced by the well-known undamped ( $\Gamma = \gamma = 0$ ) solutions of Eq. (7):<sup>21</sup>

$$2\omega_\pm^2 = \omega_p^2 + \Omega_{\text{LO}}^2 \pm [(\omega_p^2 + \Omega_{\text{LO}}^2)^2 - 4\omega_p^2 \Omega_{\text{TO}}^2]^{1/2}. \quad (9)$$

This gives rise to the LOPC upper ( $L+$ ) branch at a frequency above  $\Omega_{\text{LO}}$ , and the lower ( $L-$ ) branch below  $\Omega_{\text{TO}}$ . For  $p$ -doped GaAs, by contrast, the frequency is reproduced by the overdamped ( $\gamma > \Omega_{\text{LO}}$ ) solution of Eq. (7), which gives a phononlike coupled mode with a frequency between  $\Omega_{\text{LO}}$  and  $\Omega_{\text{TO}}$ , in addition to an overdamped plasmon mode, which

is generally too broad to appear as a distinct spectroscopic feature.<sup>22–24</sup>

Because of the formation of the depletion or accumulation layer at the surface, the LOPC mode properties can be strongly depth dependent in the surface region through the free-carrier concentration. For example, LO phonons couple with doped electron plasma in the bulk of  $n$ -doped III-V semiconductors, but remain uncoupled (unscreened) in the depletion region where the carrier concentration is low.<sup>25,26</sup>

LOPC modes can also arise from the coupling with photoinjected carriers, in addition to the impurity-doped carriers. Under high-density femtosecond laser excitation across the band gap, the free-carrier density can be significantly enhanced, modifying the LOPC frequencies and causing them to be time-dependent within the irradiated volume.<sup>27–30</sup>

### C. Raman scattering by LO phonons of zinc-blende semiconductors

Raman scattering by the LO phonon and LOPC modes of III-V compound semiconductors can have contributions from a variety of dipole-allowed and dipole-forbidden Raman scattering processes,<sup>25,26,31–38</sup> which are summarized in Table I. For the (001) surface of a zinc-blende or diamond-structure crystal, the dipole-allowed first-order Raman tensor for LO phonon scattering is the off-diagonal tensor of Eq. (4), which gives a scattering efficiency of  $|a|^2$  in the  $z(x,y)\bar{z}$  backscattering geometry and zero in the  $z(x,x)\bar{z}$  geometry. For a diamond-structure crystal, the dipole-allowed Raman polarizability  $a$  is contributed solely by that of the deformation-potential (DP) interaction  $a_{DP}$ .<sup>34</sup> In the case of a zinc-blende crystal, the polarizability associated with the linear EO effect,  $a_{EO}$ , which arises from the *interband* term of the Fröhlich interaction,<sup>26</sup> also contributes to the dipole-allowed scattering, i.e.,  $a = a_{DP} + a_{EO}$ . Since the EO effect contributes only to the LO and not to the TO phonons, the ratio of  $a_{DP}$  and  $a_{EO}$  can be experimentally obtained from the ratio of the LO and TO Raman intensities.<sup>25,26,32,33,36,37</sup> The EO contribution to the allowed scattering by the LO phonon is usually small compared with the DP contribution.<sup>26,33</sup>

For the LOPC modes of  $n$ -doped GaAs, the  $L-$  branch can be considered as being purely phononic, and its dipole-allowed Raman scattering can therefore be attributed mainly to the DP process. By contrast, the  $L+$  branch can be considered as purely plasmonic. Since no ionic deformation is present for

TABLE I. Possible mechanisms involved in the first-order resonant Raman scattering by LO and LOPC modes in III-V compound semiconductors.

Mode	Configuration	Possible mechanisms
LO	anisotropic <sup>a</sup> isotropic <sup>b</sup>	allowed DP, EO forbidden F, $F_i$ , FK <sup>c</sup>
LOPC	anisotropic <sup>a</sup> isotropic <sup>b</sup>	allowed DP, EO forbidden F, CDF <sup>d</sup> , FK <sup>c</sup>

<sup>a</sup>Corresponds to  $[z(x,y)\bar{z}]$  Raman scattering configuration.

<sup>b</sup>Corresponds to  $[z(x,x)\bar{z}]$  Raman scattering configuration.

<sup>c</sup>Efficient only in the surface depletion layer.

<sup>d</sup>Efficient only near the  $E_0$  gap.

plasmons, only the EO mechanism, which is associated with their electric field, is operative in the dipole-allowed Raman scattering.<sup>25,26</sup>

When optical excitation occurs near a critical point in the joint density of initial and final states,  $q$ -dependent Raman scattering by LO phonons can occur in dipole-forbidden geometries via the *intragap* Fröhlich (F) and Franz-Keldysh (FK) mechanisms, with  $q$  being the phonon wave vector.<sup>26</sup> Near the  $E_0$  and  $E_1$  critical points of a zinc-blende crystal, the forbidden scattering is described by a diagonal tensor of Eq. (5), which gives a scattering efficiency of  $|b|^2$  in the  $z(x,x)\bar{z}$  scattering geometry and zero in the  $z(x,y)\bar{z}$  geometry. The dipole-forbidden Raman polarizability  $b$  can be written as the sum of the polarizabilities due to the F and FK mechanisms, i.e.,  $b = a_F + a_{FK}$ . The scattering cross section of F coupling is proportional to the square of the momentum transfer  $q^2$ ; it shows a sharp resonance behavior at the  $E_0$  gap.<sup>33</sup> The LO phonons most contributing to the F scattering have a wave vector  $q \simeq 0.04/a_0$  for undoped GaAs at the  $E_0 + \Delta_0$  gap, where  $a_0$  is the lattice constant.<sup>34</sup> The FK mechanism is responsible for electric-field-induced Raman scattering in the presence of a strong electric field.<sup>26</sup> The FK mechanism is important in the near-surface regions of doped compound semiconductors, which can have strong built-in fields in the surface depletion or accumulation layers of tens of nanometers thickness.

Dipole-forbidden Raman scattering by LOPC mode is also contributed by the charge-density fluctuation (CDF) for semiconductors with carriers at the zone center.<sup>32</sup> The dipole-forbidden polarizability for the LOPC mode is thus given by  $b = a_F + a_{FK} + a_{CDF}$ , with  $a_{CDF}$  being the polarizability due to the CDF interaction.<sup>25</sup> In CDF, intragap transitions occur via Fröhlich interaction between the longitudinal electric field of the coupled modes and charge carriers.<sup>36</sup> CDF is therefore efficient at the  $E_0$  resonance, where the amount of free carriers occupying the conduction band minimum is large; it is unimportant near the  $E_1$  resonance, where the carrier density in the  $L$  valleys is negligible.<sup>26</sup> The FK effect can be effective for the LOPC modes within the depletion or accumulation layer of doped semiconductors; for those arising from the bulk, however, it should be negligible because of the absence of a strong internal field.

In addition to the intrinsic Raman scattering mechanisms described above, extrinsic impurity-induced Fröhlich ( $F_i$ ) scattering with polarizability  $a_{F_i}$ ,

$$\vec{R}_{F_i} = \begin{pmatrix} a_{F_i} & 0 & 0 \\ 0 & a_{F_i} & 0 \\ 0 & 0 & a_{F_i} \end{pmatrix}, \quad (10)$$

has been found for the LO phonon of compound semiconductors.<sup>34</sup>  $F_i$  is incoherent with respect to the intrinsic mechanisms, because it terminates at a different final state with a broader distribution of  $q$ . In this scattering process, an electron is scattered twice, once through carrier-phonon and again through carrier-impurity interaction. Nevertheless, owing to the  $q^2$  dependence of the scattering cross sections as well as to the double resonance,  $F_i$  can be very efficient. It is even more efficient than the F coupling for undoped GaAs near the  $E_0$  resonance, because the LO phonons most contributing to the  $F_i$  scattering have a wave vector  $q \simeq 0.2/a_0$ , significantly larger than those contributing to the F

scattering.<sup>34,35</sup>  $F_i$  is strong in undoped bulk or depleted surface layer due to the unscreened impurities, but it should be weak in heavily doped bulk because of the screening of the impurity potential.<sup>25,26</sup>

### III. EXPERIMENTAL

The samples studied are (001)-orientated nominally undoped GaAs (*i*-GaAs) and *n*-type GaAs doped with  $\sim 1 \times 10^{18} \text{ cm}^{-3}$  Si (*n*-GaAs). The maximum thickness of the depletion layer of the *n*-GaAs sample is estimated to be 40 nm.<sup>39</sup> As a reference, we also measure In-doped Ge(001) for which we expect the allowed DP Raman scattering to contribute exclusively in both generation and detection. The comparison of GaAs results with Ge provides an estimate of potential systematic experimental errors due to the incomplete back-reflection configuration and polarization leakage.

Pump-probe reflectivity measurements are performed at room temperature under ambient conditions. The fundamental output from a Ti:sapphire oscillator with 30-fs duration, 1.55 eV (800-nm) energy, and 80-MHz repetition rate is used to excite GaAs samples near the  $E_0$  critical point. Either the fundamental or the second harmonic at 3.1 eV (400 nm) generated in a  $\beta$ -BaB<sub>2</sub>O<sub>4</sub> (BBO) crystal is used to probe the optical response near the  $E_0$  or  $E_1$  critical points (1.42 and 2.92 eV at room temperature<sup>41</sup>). Possible interband transitions with the probe photons are illustrated in Fig. 1. Linearly polarized pump and probe beams are incident on the sample surface with angles of  $<5^\circ$  and  $<15^\circ$  from the surface normal. The maximum photoexcited carrier densities are estimated to be  $1.6 \times 10^{18} \text{ cm}^{-3}$  for the degenerate experiments and  $2.6 \times 10^{17} \text{ cm}^{-3}$  for the two-color experiments. The probe beam is monitored before and after reflection from the sample with a pair of matched photodiodes, and their signals are subtracted in order to minimize the noise due to the laser

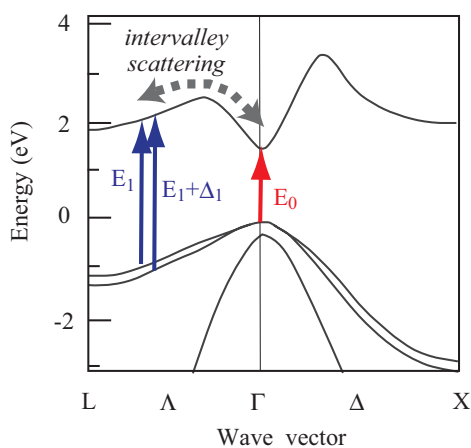


FIG. 1. (Color online) Schematic band structure of GaAs near the fundamental band gap.<sup>40</sup> Major transitions with 1.55 and 3.1 eV photons are designated with vertical arrows. 1.55 eV light is nearly resonant with the  $E_0$  critical point at 1.42 eV, whereas 3.1 eV light is nearly resonant with the  $E_1$  and  $E_1 + \Delta_1$  critical points at 2.92 and 3.14 eV at room temperature.<sup>41</sup> The broken arrow indicates the  $\Gamma$ -L intervalley scattering<sup>42</sup> that is responsible for the delayed rise of the reflectivity change in the two-color scheme [see Fig. 3(b)].

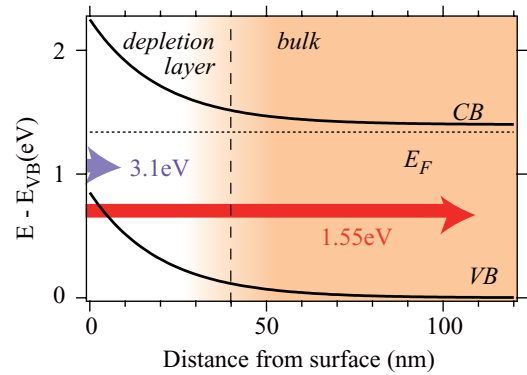


FIG. 2. (Color online) Comparison of probe depths for the 1.55 and 3.1 eV light with the thickness of the depletion layer of *n*-type GaAs ( $n_{\text{dope}} = 1 \times 10^{18} \text{ cm}^{-3}$ ).<sup>39</sup> Probe depths, determined as described in the text, are indicated by the length of the horizontal arrows. The band-bending magnitude before photoexcitation is also schematically plotted, with CB and VB denoting the conduction band minimum and valence band maximum, respectively.

intensity fluctuations. For the coherent phonon detection, time delay between pump and probe pulses is modulated at 20 Hz to achieve accumulation and averaging with a digital oscilloscope (fast scan). For measurement of the reflectivity change due to the photoexcited carriers, which decays on the picosecond and longer time scales, the time delay is scanned with a computer-controlled translational stage (slow scan).

The IR and UV probe measurements differ significantly in their probing depths. In the case of 1.55 eV light, the probing depth is determined by the reflection depth of a transparent medium  $\lambda/2n \simeq 110 \text{ nm}$ , where  $n = 3.7$  is the refractive index,<sup>43</sup> because the absorption depth is longer. For the more strongly absorbing 3.1 eV light, the probing depth is given by one half of the penetration depth  $1/2\alpha = 7.5 \text{ nm}$  ( $\alpha$  is the absorption coefficient), because the reflected probe light transverses the sample twice. Compared with the depletion layer thickness of *n*-GaAs, indicated in Fig. 2, the 1.55 eV light probes both the bulk and depletion-layer response, whereas the 3.1 eV light probes exclusively the depletion region.

## IV. RESULTS

### A. Pump-power dependence of transient reflectivity at the $E_0$ gap

We first examine the electronic response of GaAs samples. A trace of pump-induced reflectivity change ( $\Delta R/R$ ) acquired in the slow-scan mode for *n*-GaAs is shown in Fig. 3(a) for pumping and probing at 1.55 eV.  $\Delta R/R$  increases within 300 fs to a maximum value  $A_{\text{el}}$  and decays multiexponentially on the picosecond and slower time scales. The reflectivity of *i*-GaAs (not shown) evolves similarly, except that the decay is dominated by a fast ( $<5 \text{ ps}$ ) decaying component. For both samples, the rise reflects the interband excitation of carriers near the  $E_0$  gap, and the decay shows their relaxation via inter- and intervalley scattering, optical-phonon emission, and recombination, which occur from the subpicosecond to the nanosecond time scales.<sup>42</sup>

The fast scan of the delay enables detection of small amplitude coherent oscillations, which are superimposed on

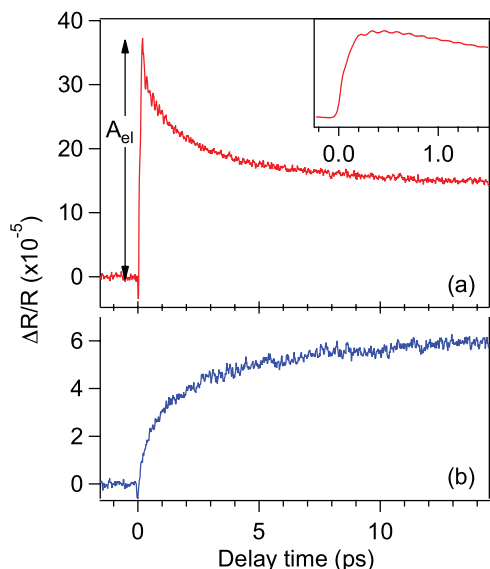


FIG. 3. (Color online) Reflectivity change from  $n$ -GaAs (001) obtained from a slow scan of pump-probe delay; (a) with pump and probe at 1.55 eV, (b) with pump at 1.55 eV and probe at 3.1 eV.  $A_{el}$  in (a) denotes the maximum reflectivity change induced by the pump pulse. Inset in (a) shows the first picosecond of the transient response measured with the fast-scan method.

the much larger amplitude nonoscillatory reflectivity change, as shown in the inset of Fig. 3(a). Figure 4(a) shows the oscillatory part of  $\Delta R/R$  of the  $n$ -GaAs samples after subtraction of a double exponential function that is used to model the nonoscillatory response. The pump-fluence dependence of the coherent response is most conveniently seen in the spectrum in Fig. 4(b) obtained by performing a Fourier transform (FT) on the time-domain signal. The FT spectrum is dominated by an intense peak at 7.6 THz, which was attributed to the  $L-$  branch of the LOPC mode from the  $n$ -doped bulk in previous transient reflectivity studies.<sup>29,30</sup> We also observe a weak, broad peak at  $\sim 11$  THz due to the  $L+$  branch from the bulk as well as the bare (unscreened) LO phonon peak from the surface depletion layer at 8.7 THz, also in agreement with the previous studies.<sup>29,30</sup> The unscreened LO phonon appears either as a negative or a positive peak in the FT spectrum [see Fig. 4(b)], depending on the polarization of the pump and probe beams and the time range used in the FT.<sup>44</sup>

The oscillatory reflectivity signal can be fitted to a sum of damped harmonic oscillators, each of which is described by<sup>45</sup>

$$\frac{\Delta R(t)}{R} = \frac{\Delta R(t=0)}{R} \exp(-\Gamma t) \sin(2\pi \Omega t + \psi). \quad (11)$$

The  $L-$  frequency obtained from the time-domain fitting upshifts slightly with pump fluence, whereas the LO frequency is independent of pump fluence, as shown in Fig. 4(c). The upshift is reproduced by the solid curves in the same panel, which represent the undamped LOPC frequencies given by Eq. (9) for the carrier density  $n$  taken as the sum of the doped and photoexcited carrier densities ( $n = n_{dope} + n_{exc}$ ).<sup>29</sup> The  $L-$  amplitude increases sublinearly with increasing pump density, in rough accordance with  $A_{el}$ , as shown in Fig. 4(d). The correlation suggests that the generation of the coherent  $L-$  mode is directly related to the photocarrier density, which

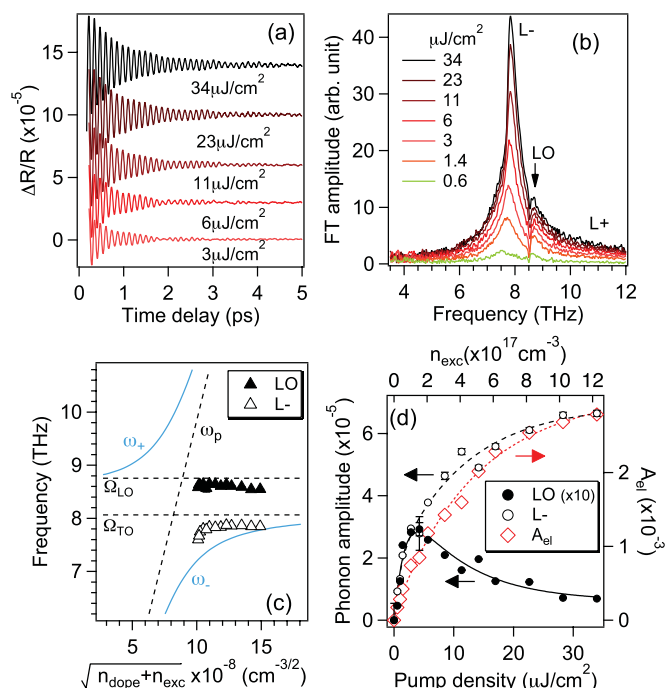


FIG. 4. (Color online) (a) The oscillatory parts of the transient reflectivity  $\Delta R/R$  response and (b) their FT spectra of  $n$ -GaAs (001) pumped and probed with 1.55 eV light at different pump densities. Pump and probe polarizations are perpendicular and parallel to the [110] axis. Traces in (a) are offset for clarity. (c) LO and LOPC frequencies as a function of the carrier density  $n = n_{dope} + n_{exc}$ . Solid curves represent the LOPC frequencies calculated with Eq. (9). (d) Amplitudes  $\Delta R(t=0)/R$  of LO phonon,  $L-$  mode (left axis), and  $A_{el}$  (right axis) as a function of pump density. The vertical scale for the LO amplitude is magnified ten times. Curves are to guide the eye.

is proportional to  $A_{el}$ . By contrast, the bare LO amplitude reaches maximum at a very low excitation density of  $\sim 1.8 \times 10^{17} \text{ cm}^{-3}$  and then decreases, indicating a complex relationship between its generation and the photocarrier density.

The coherent response of  $i$ -GaAs [see Figs. 5(a) and 5(b)] is found to be substantially different from  $n$ -GaAs, indicating an important role of the doped carriers. At low fluence below  $5 \mu\text{J}/\text{cm}^2$ , the FT spectrum [see Fig. 5(b)] is dominated by the sharp peak of the bare LO phonon at 8.7 THz from the undoped bulk, in agreement with a previous study on undoped GaAs.<sup>7</sup> By increasing pump fluence, however, we find broader peaks grow in below  $\Omega_{TO}$  and above  $\Omega_{LO}$ , which were not reported previously. The frequencies of both peaks upshift with pump fluence, which can be reproduced reasonably in Eq. (9) by setting  $n = n_{exc}$  [see Fig. 5(c)]. We therefore attribute the broad peaks to the  $L-$  and  $L+$  branches of the LOPC mode associated with the *photoexcited* electron plasma in the undoped bulk sample.<sup>46</sup> Unlike the  $n$ -GaAs, the amplitude of the coherent LO phonon increases sublinearly with pump fluence, in accordance with  $A_{el}$  [see Fig. 5(d)], indicating the direct relation between the generation and the photoexcited carrier density.

## B. Pump-polarization dependence at the $E_0$ gap

Kurz and coworkers examined the generation mechanisms of the coherent phonons in GaAs by changing the surface

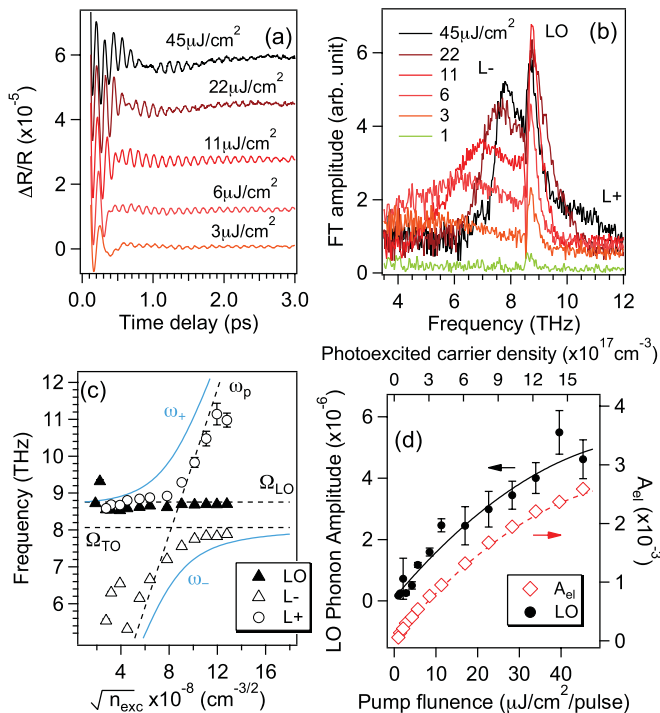


FIG. 5. (Color online) (a) The oscillatory parts of  $\Delta R/R$  response and (b) their FT spectra of *i*-GaAs (001) pumped and probed with 1.55 eV light at different pump fluences. Pump and probe polarizations are perpendicular and parallel to the [110] axis of the crystal. Traces in (a) are offset for clarity. (c) LO and LOPC frequencies as a function of photoexcited carrier density  $n = n_{\text{exc}}$ . Solid curves represent the frequencies calculated with Eq. (9). (d) LO phonon amplitude (left axis) and  $A_{\text{el}}$  (right axis) as a function of pump fluence. Curves are to guide the eye. Zeros of the left and right axes are offset for clarity.

fields with external voltage.<sup>8,9</sup> The dependence of the phonon amplitude on the applied field was consistent with the TDFS excitation mechanism. Here, we reexamine the generation mechanism by measuring the coherent response for different polarization angles  $\phi$  of the pump light. We report the *initial amplitude*  $\Delta R(t=0)/R$  of each phonon mode, instead of its FT peak intensity done in the previous studies<sup>20,47</sup> because the former also gives the phase information.

Figure 6 presents the amplitudes of the coherent LO and LOPC modes of GaAs samples as well as that of the optical phonon of Ge, as a function of  $\phi$  measured with respect to the [110] crystallographic axis. Table II summarizes the anisotropy  $|B|/(|A| + |B|)$  in the coherent amplitudes from a fit to  $A + B \cos 2\phi$ . The amplitude of the optical phonon of Ge, whose generation is contributed exclusively by ISRS via allowed DP scattering, exhibits the expected  $\cos 2\phi$  dependence.<sup>17</sup> The experimentally obtained anisotropy of near unity ( $0.98 \pm 0.02$ ) indicates that systematic errors due to the imperfect back-reflection configuration and polarization leakage can be neglected.

We find the LO and LOPC amplitudes of *n*-GaAs to be independent of  $\phi$ , in agreement with a previous transient reflectivity study,<sup>8</sup> and thereby confirm the TDFS generation.<sup>1,2</sup> For *i*-GaAs, by contrast, the amplitudes of the LO phonon [see Fig. 6(a)] and LOPC mode (not shown) exhibit a clear

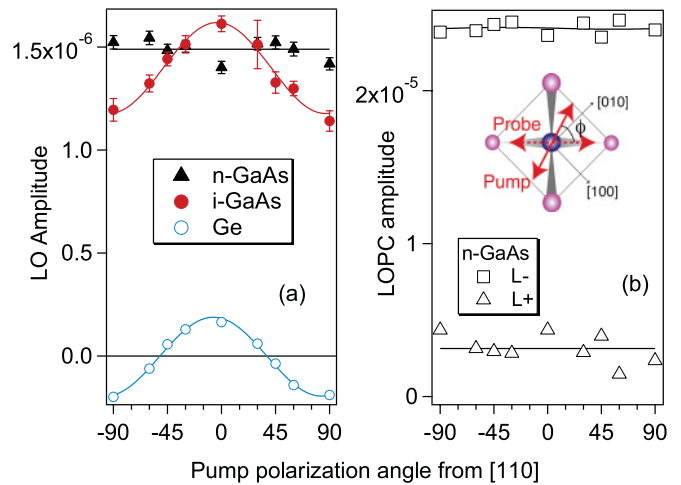


FIG. 6. (Color online) Pump-polarization dependence of the initial amplitudes of coherent phonons pumped and probed at 1.55 eV: (a) LO phonon of GaAs and optical phonon of Ge and (b) LOPC mode of *n*-GaAs. Inset of (b) shows the polarization of pump and probe beams with respect to the crystal. Polarization of probe is fixed to be parallel to the [110] axis, and the pump polarization angle  $\phi$  is rotated with respect to it. Solid curves show the fitting to  $A + B \cos 2\phi$ .

dependence on  $\phi$ , which can be fitted to the  $A + B \cos 2\phi$  function. The coexistence of  $\phi$ -independent and  $\phi$ -dependent amplitudes indicates contributions from both TDFS<sup>7,8</sup> and dipole-allowed ISRS generation mechanisms.<sup>20</sup> We note that the coherent mode frequencies and dephasing rates show no systematic dependence on  $\phi$ .

The  $\phi$ -independent LO phonon amplitude ( $A$ ) is comparable for *n*-GaAs and *i*-GaAs [see Fig. 6(a)]. This does not mean that the TDFS generation efficiency is comparable for the two crystals, however, because the unscreened LO phonon of *n*-GaAs arises from a much smaller volume (only the depletion layer) than that of *i*-GaAs (the entire probe depth). To yield comparable amplitudes, the TDFS generation in *n*-GaAs must be more efficient than in *i*-GaAs as we will discuss further in Sec. V A. The similarity between the anisotropic amplitude ( $B$ ) of *i*-GaAs and Ge [see Fig. 6(a)] also is fortuitous, because the photoexcitation at 1.55 eV occurs for a

TABLE II. Anisotropy  $[|B|/(|A| + |B|)]$  in the pump-polarization dependence of the coherent amplitudes of GaAs and Ge, obtained from fitting the data in Fig. 6 to  $A + B \cos 2\phi$ . Dominant generation mechanisms are also listed.

Sample	Mode	Anisotropy	Generation mechanism
<i>n</i> -GaAs	LO (depletion layer)	<0.03	TDFS
	<i>L</i> - (bulk)	<0.01	TDFS
	<i>L</i> + (bulk)	<0.3	TDFS
<i>i</i> -GaAs	LO (bulk)	0.14	TDFS > ISRS
	<i>L</i> - (bulk)	<0.2	TDFS
	<i>L</i> + (bulk)	<0.1	TDFS
Ge	optical phonon	0.98	ISRS

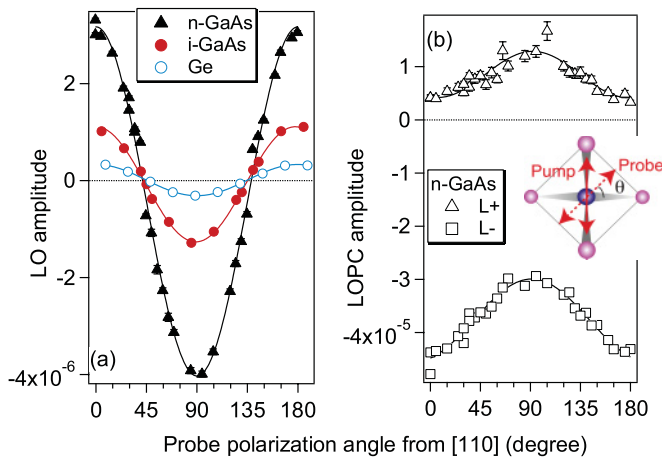


FIG. 7. (Color online) Probe-polarization dependence of amplitude of coherent phonons pumped and probed at 1.55 eV: (a) coherent LO phonon of GaAs and optical phonon of Ge and (b) LOPC mode of *n*-GaAs. Polarization of pump is parallel to the  $[1\bar{1}0]$  axis, and the probe polarization angle  $\theta$  is rotated with respect to the  $[110]$  axis. Solid curves show the fitting to  $C + D \cos 2\theta$ .

different range of wave vectors in the band structures of the two materials.

### C. Probe-polarization dependence near the $E_0$ gap

We next investigate the coherent phonon detection mechanisms through the dependence of the oscillatory signal on the polarization angle  $\theta$  of the probe light. Figure 3 shows plots of the initial amplitude  $\Delta R(t=0)/R$  as a function of  $\theta$  with respect to the  $[110]$  crystallographic axis for the GaAs and Ge samples. Table III summarizes the anisotropy  $|D|/(|C| + |D|)$  in the amplitude of the coherent response when fitted to  $C + D \cos 2\theta$ . The measured Ge optical phonon anisotropy of  $0.97 \pm 0.01$  is in agreement with the previous transient reflectivity study, which explained the observed  $\cos 2\theta$  dependence in terms of the anisotropic band-gap modulation through the DP interaction.<sup>17,18</sup> The  $\cos 2\theta$  dependence can also be interpreted in terms of the symmetry of the off-diagonal allowed Raman tensor  $\partial\chi/\partial Q$  [see Eq. (4)] involved in

TABLE III. Anisotropy  $[|D|/(|C| + |D|)]$  in the probe-polarization dependence of the coherent phonon amplitudes of GaAs and Ge near the  $E_0$  gap, obtained from fitting the data in Fig. 7 to  $C + D \cos 2\theta$ . Dominant Raman scattering mechanisms in the detection process are also listed.

Sample	Mode	Anisotropy	Detection mechanism
<i>n</i> -GaAs	LO (depletion layer)	0.87	DP > $F_i$ + FK
	$L^-$ (bulk)	0.15	CDF > DP
	$L^+$ (bulk)	0.34	CDF > EO
<i>i</i> -GaAs	LO (bulk)	0.94	DP
	$L^-$ (bulk)	<0.2	CDF
	$L^+$ (bulk)	<0.3	CDF
Ge	optical phonon	0.97	DP

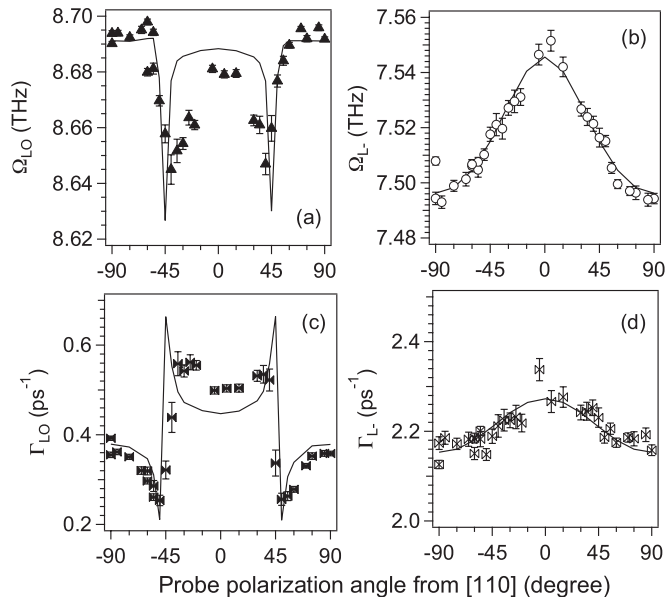


FIG. 8. (a) The frequency of the LO phonon, and (b) the  $L^-$  mode as well as (c) the dephasing rate of the LO phonon, and (d) the  $L^-$  mode of *n*-GaAs measured as a function of the probe-polarization angle  $\theta$  with respect to the  $[110]$  axis. Polarization of pump is parallel to the  $[1\bar{1}0]$ . Pump and probe light is at 1.55 eV. Solid curves represent the fitting results to a model function given by Eq. (13), with parameters described in the text.

the reflectivity modulation  $\Delta R$  by nuclear displacement  $Q$  [see Eq. (6)]. The experimentally obtained anisotropy of Ge confirms that the systematic experimental uncertainties in the reflectivity anisotropies are insignificant also in our probe-polarization dependence measurements.

We interpret the LO phonon anisotropy of 0.94 for *i*-GaAs, which is in agreement with a previous study on undoped GaAs at 2 eV,<sup>7</sup> to imply the dominant DP detection mechanism, just like for Ge. By contrast, for the LO phonon of *n*-GaAs, we find a minor but indubitable isotropic contribution ( $C \neq 0$ ). Furthermore, the  $L^-$  and  $L^+$  modes exhibit larger isotropic amplitudes than the anisotropic ones, i.e.,  $C > D$  for both *i*-GaAs and *n*-GaAs samples, which is consistent with the previous report for *n*-type GaAs with 1.47 eV pump-probe photon energy.<sup>16</sup> We attribute the isotropic amplitude  $C$  to the reflectivity modulation via the dipole-forbidden Raman scattering, whose Raman tensor is diagonal [see Eq. (5)]. The Raman scattering cross sections of the forbidden processes are known to be enhanced sharply at  $E_0$  and  $E_1$  resonances to such an extent that they can be comparable or larger than those of the allowed processes.<sup>25,33–35,37</sup>

Besides the component amplitudes, both the coherent LO and  $L^-$  modes of *n*-GaAs show an anisotropy in their frequencies and dephasing rates, as shown in Fig. 8. A similar anisotropy was reported for the dephasing rate of the coherent  $L^-$  mode of *n*-doped GaAs,<sup>16</sup> but not reported for its frequency or for those of the LO phonon. We have confirmed that the corresponding anisotropy is indiscernible for *i*-GaAs or Ge (not shown), and therefore is not an experimental artifact. We will discuss the origin of the anisotropy in Sec. V E.

### D. Pump near the $E_0$ gap and probe near the $E_1$ gap

Next, we investigate the transient reflectivity response when the probe photon energy is 3.1 eV, i.e., at resonance with the  $E_1$  gap, while maintaining the pump at 1.55 eV. By contrast to 1.55 eV probing, the nonoscillatory reflectivity change due to photoexcited carriers has a delayed rise on the picosecond time scale, as shown in Fig. 3(b). This is because the 1.55 eV light excites carriers in the  $\Gamma$  valley, whereas 3.1 eV light probes hot electrons and holes with large momenta along the  $\Gamma$ - $L$  line that are produced by thermalization of the nascent  $\Gamma$  valley carrier distribution (see Fig. 1). For longer delays, the reflectivity decreases on subnanosecond time scale (not shown) due to carrier-lattice equilibration and transport.<sup>42</sup>

Figure 9(a) shows the oscillatory part of  $\Delta R/R$  response of  $n$ -GaAs for the two-color pump-probe scheme, with pump and probe polarizations parallel to the [110] crystallographic axis.<sup>48</sup> By contrast to the one-color results in Fig. 4, the oscillation is dominated by the unscreened LO phonon at 8.7 THz; the intense  $L$ - mode at 7.6 THz is absent, as seen in the FT spectrum in Fig. 9(b). Instead, the LO peak is accompanied by a shoulder at  $\sim 8.2$  THz, which was not present with the 1.55 eV probing. The difference in the coherent response with respect to 1.55 eV probing can be attributed primarily to the fact that the 3.1 eV light monitors only the depletion layer (see Fig. 2), in which the LO phonons are mostly unscreened.

The amplitude, dephasing rate, and frequency of the unscreened LO phonon are independent of the pump fluence according to Fig. 10. The fluence-insensitive LO amplitude was also observed for  $n$ -GaAs in a previous time-resolved second harmonic generation (TR-SHG) study, and attributed to complete screening of the depletion field at photoexcited carrier density of  $n_{\text{exc}} < 1 \times 10^{17} \text{ cm}^{-3}$ .<sup>49</sup> By contrast, the amplitude of the  $\sim 8.2$  THz shoulder grows linearly [see Fig. 10(a)]. In fact, this oscillatory component is better

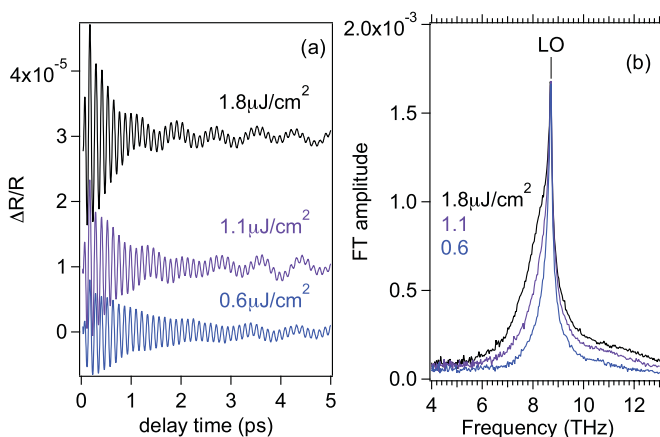


FIG. 9. (Color online) (a) The oscillatory part of  $\Delta R/R$  response and (b) their FT spectra for the  $n$ -GaAs (001) pumped at different densities at the  $E_0$  gap with 1.55 eV light and probed at the  $E_1$  gap with 3.1 eV light. Pump and probe polarizations are parallel to the [110] axis. Traces in (a) are offset for clarity.

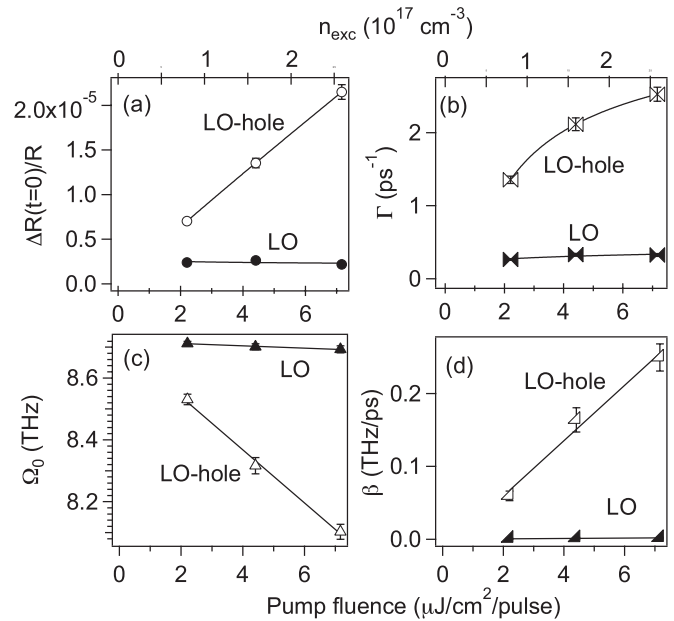


FIG. 10. Pump-fluence dependence of the (a) amplitude, (b) dephasing rate, (c) frequency, and (d) chirp of the LO (filled symbols) and LO-hole coupled (open symbols) modes of the  $n$ -GaAs pumped at 1.55 eV and probed at 3.1 eV. Pump and probe polarizations are parallel to the [110] axis. Solid curves are to guide the eye.

described as a linearly chirped damped harmonic oscillation:

$$\frac{\Delta R(t)}{R} = \frac{\Delta R(t=0)}{R} \exp(-\Gamma t) \sin[2\pi(\Omega_0 + \beta t)t + \psi], \quad (12)$$

with the frequency increasing with time at a rate  $\beta$ , rather than by Eq. (11). Both the initial redshift of the frequency [see Fig. 10(c)] and its subsequent blueshift with delay [see Fig. 10(d)] become larger for higher pump fluences. The fluence dependence suggests that the  $\sim 8.2$  THz mode is a phonon-plasmon coupled mode involving the photoexcited carriers. Its frequency between  $\Omega_{\text{LO}}$  and  $\Omega_{\text{TO}}$ , however, is not expected from the LO phonon-electron plasma-coupled mode modeled by Eq. (9). Similar “anomalous” LOPC frequency was reported in a TR-SHG study on  $n$ -GaAs, and assigned as the LO phonons coupled with photoexcited hole plasma within the depletion layer.<sup>50</sup> Here, we assign the  $\sim 8.2$ -THz mode to the similar LO-hole plasmon-coupled mode, and will discuss it further in Sec. VD.

Varying the probe-polarization angle  $\theta$  changes the appearance of the coherent oscillation drastically, as seen in the FT spectrum in Fig. 11(a). We notice that, when the probe polarization is nearly perpendicular to the [110] axis, a third, weak, and fast-decaying component appears at  $\sim 6.7$  THz. We assign this additional feature to LO phonon coupling with the photoinduced electron plasma, which was also observed in the TR-SHG study.<sup>50</sup> Its frequency, which is significantly lower than that of the  $L$ - mode observed with the 1.55 eV probe, can be attributed to the much lower doped electron density in the depletion layer than in the bulk of  $n$ -GaAs. The LO-, LO-hole-, and LO-electron-mode amplitudes can be fit to the  $C + D \cos 2\theta$  form, as shown in Fig. 11(b).

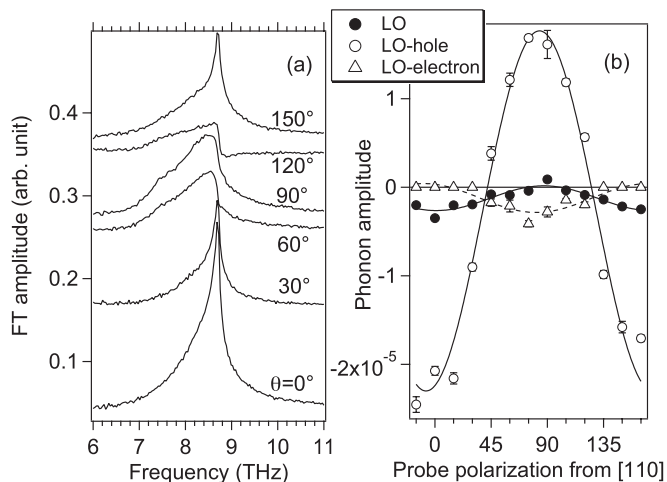


FIG. 11. Probe-polarization dependence of the (a) FT spectrum of the oscillatory reflectivity and (b) the amplitudes of the coherent oscillations of the  $n$ -GaAs pumped at 1.55 eV and probed at 3.1 eV. Pump polarization is parallel to the [110] axis, and the probe polarization angle  $\theta$  is rotated with respect to it. Solid curves in (b) show fitting to  $C + D \cos 2\theta$ .

Table IV summarizes the anisotropy  $|D|/(|C| + |D|)$  in the amplitude of the coherent response. The LO (LO-electron) amplitude nearly vanishes at  $\theta \sim 90^\circ$  ( $0^\circ$ ), which implies  $C \simeq D$  ( $C \simeq -D$ ). For the LO-hole amplitude, the isotropic contribution is much smaller than the anisotropic one, i.e.,  $|C| \ll |D|$ . We will discuss the obtained anisotropies in terms of the allowed and forbidden Raman scattering processes in Sec. VD.

We are not able to analyze the  $\theta$  dependence of the frequencies and dephasing rates of the coherent modes in the two-color experiments, because the three (rather than two) frequencies are not well separated, and most likely undergo a chirp with the delay. Next, we discuss the mechanisms for generation and detection of the coherent modes of GaAs.

## V. DISCUSSION

### A. Generation mechanism of LO and LOPC modes

The anisotropy in the generation of coherent phonons is summarized in Table II. The vanishing anisotropy for  $n$ -GaAs indicates that the generation of both coherent LO and LOPC modes is dominated by TDFS, in agreement with early studies that reported on the  $L-$  mode of  $n$ -doped GaAs.<sup>7-9</sup> Our results confirm that ultrafast carrier separation by the built-in field in the depletion layer launches not only coherent LO phonons within the depletion layer of  $n$ -GaAs, but also coherent LOPC modes in the adjacent bulk via ultrafast drift-diffusion current.<sup>1,2,8</sup> The dominance of the TDFS generation mechanism can explain the distinct power dependence of the LO amplitude in  $n$ -GaAs [see Figs. 4(d) and 10(a)]. We expect the TDFS generation within the depletion layer to saturate above a critical carrier density at which point the band bending is fully screened. This happens for  $n$ -GaAs at a density of  $n_{\text{exc}} < 2 \times 10^{18} \text{ cm}^{-3}$  for 1.55 eV probe and at even smaller density for 3.1 eV probe [see Fig. 10(a)]. The difference can be attributed to the higher effective density of photoexcited

TABLE IV. Anisotropy  $[|D|/(|C| + |D|)]$  in the probe-polarization dependence of the coherent phonon amplitudes of  $n$ -GaAs near the  $E_1$  gap, obtained from fitting the data in Fig. 11 to  $C + D \cos 2\theta$ . Dominant Raman scattering mechanisms in the detection process are also listed.

Mode	Anisotropy	Detection mechanism
LO (depletion layer)	0.53	DP $\sim$ FK
LO-hole (top depletion layer)	0.88	DP $>$ FK
LO-electron (deeper depletion layer)	0.57	DP $\sim$ FK

holes near the surface, which is probed by 3.1 eV light, than the average over the whole depletion layer probed by 1.55 eV light, as a result of the ultrafast drift-diffusion. Meanwhile, the LOPC amplitude of  $n$ -GaAs keeps increasing even after the saturation of the LO amplitude [see Fig. 8(d)], because the generation of the bulk mode is not limited by the screening of the surface field.

For the bulk LO phonon of  $i$ -GaAs, we find a small contribution from ISRS generation mechanism in addition to the dominant TDFS. Our finding that even in  $i$ -GaAs coherent LO phonons are generated via TDFS rather than ISRS may be surprising, but is consistent with the previous study, in which a prepulse was used to screen the surface field and thereby reduce the amplitude of the coherent LO phonon of undoped GaAs.<sup>7</sup> Fermi level pinning by acceptor-type surface defects lying  $\sim 0.5$  eV above the valence band maximum<sup>51</sup> can produce a band bending required for TDFS also in  $i$ -GaAs, though it is weaker than that in  $n$ -GaAs. For  $i$ -GaAs, generation of coherent LO phonons via the TDFS mechanism is only six times more efficient than via the allowed ISRS mechanism, according to the anisotropy in the excitation process, because of the weak surface built-in field. For  $n$ -GaAs, by contrast, the experimentally obtained anisotropy of  $< 0.03$  indicates that TDFS is at least 30 times larger than ISRS, because of the strong surface field. Unlike  $n$ -GaAs, the LO amplitude of  $i$ -GaAs [see Fig. 5(d)] does not show a clear saturation with increasing pump power. The difference between the two GaAs samples can be attributed to the fact that the complete screening of the built-in field in  $i$ -GaAs requires higher carrier density because of the smaller drift velocity due to weaker built-in field.

In principle, dipole-forbidden ISRS can also contribute to the  $\phi$ -independent generation of coherent phonons, as was suggested for GaAs/AlGaAs multiple quantum wells.<sup>20</sup> For the unscreened LO phonon, however, the probe-polarization dependence in Fig. 7(a) indicates a significantly smaller contribution from the forbidden Raman scattering than the allowed scattering. Because the allowed ISRS generation is small compared with TDFS [see Fig. 6(a)], we can reasonably neglect the forbidden ISRS in the excitation of the LO phonon mode. We can likewise conclude from the absence of the allowed ISRS mechanism [see Fig. 6(b)] in the generation of the  $L-$  ( $L+$ ) mode that the isotropic forbidden ISRS is unlikely to have a significant contribution, because in detection it is no more than six times (twice) as large as the allowed ISRS [see Fig. 7(b)].

### B. Detection mechanisms of LO phonons

We attribute the anisotropic and isotropic amplitudes in the detection [see Figs. 7 and 11] to the action of the lattice or electronic polarization on the reflected probe light through dipole-allowed and dipole-forbidden Raman scattering processes, respectively. This assignment can explain different anisotropy for different coherent modes and probe wavelengths.

The anisotropy of the unscreened LO phonon for the 1.55 eV probe [see Table III] is close to unity, both for  $n$ -GaAs and  $i$ -GaAs, indicating that the allowed Raman scattering dominates over the forbidden scattering. This is consistent with a previous Raman study, which found that the forbidden scattering had a very narrow resonance at the  $E_0$  gap.<sup>33</sup> Based on the resonant Raman studies,<sup>26,33</sup> we attribute the allowed Raman scattering by the LO phonon primarily to the DP interaction.

According to the resonant Raman studies, the forbidden scattering by LO phonon at the  $E_0$  gap is a consequence of the predominantly extrinsic  $F_i$  interaction rather than the intrinsic  $F$  interaction.<sup>34,35</sup> We therefore attribute the small forbidden Raman scattering mainly to the  $F_i$  mechanism. Though the theory of resonant Raman scattering treats extrinsic  $F_i$  scattering as incoherent with respect to other intrinsic scattering mechanisms, it can still contribute to the generation and detection of coherent phonons. Indeed, the defect-induced (D) mode of carbon nanotubes and graphite, which involves a similar double resonance, was also observed as a coherent modulation of the reflectivity,<sup>52,53</sup> demonstrating the possibility of classical coherence of such extrinsic scattering processes.

The anisotropy of the LO phonon detection for  $n$ -GaAs is slightly smaller than for  $i$ -GaAs at 1.55 eV. This difference can be attributed to the FK effect for the depletion layer of  $n$ -GaAs, making a larger forbidden scattering.<sup>26,54–56</sup> The anisotropy of the LO phonon becomes significantly smaller when we probe  $n$ -GaAs with 3.1 eV light, indicating that the forbidden scattering is as strong as the allowed scattering [see Table IV]. The strong forbidden scattering reflects strong sensitivity of the 3.1 eV light to the surface [see Fig. 2] where the FK effect is more effective.

### C. Detection mechanisms of LOPC mode

The anisotropy in the detection of the LOPC modes can be understood in the similar manner as that of the LO phonon. When probed at 1.55 eV, the anisotropy [see Table III] of the LOPC mode is considerably smaller than unity for both  $i$ - and  $n$ -GaAs, indicating that the dipole-forbidden Raman scattering dominates. The forbidden scattering by the bulk LOPC mode has contributions from the CDF and  $F$  interactions.<sup>25,26,32,36,37</sup> We expect large CDF interaction near the  $E_0$  gap, because both doped and photoexcited carriers at the zone center can contribute efficiently.<sup>25,37,57</sup>  $F$  mechanism, by contrast, is known to be weaker than CDF for 1.55 eV probing,<sup>25,32,37</sup> though exactly at the  $E_0$  critical point (1.42 eV at room temperature) it is comparable to CDF.<sup>36</sup> We therefore conclude that CDF is responsible for the large forbidden scattering for both the  $L-$  and  $L+$  branches.  $F_i$  and FK effects are negligible for LOPC mode in the heavily doped bulk, because of the screening of the impurity potential and

because of the absence of strong surface field, respectively. The small anisotropic allowed scattering by the  $L+$  and  $L-$  branches can be attributed to the EO and DP mechanisms, respectively, because the two branches can be treated as being purely plasmonic and phononic.<sup>25,26</sup>

When probed with 3.1 eV light, the anisotropy of the LOPC (LO-hole and LO-electron) modes [see Table IV] increases significantly compared with the 1.55 eV probe, indicating relatively smaller contribution from the forbidden Raman scattering than at 1.55 eV. This result supports our assignment of the forbidden scattering at the  $E_0$  gap to the CDF mechanism, which is not operative at the  $E_1$ .<sup>26,57–59</sup> The forbidden scattering for 3.1 eV probing is attributed primarily to the FK effect due the strong surface field in the depletion layer. The forbidden contribution for the LO-hole mode is smaller than that for the LO-electron mode, presumably because the strength of the FK effect decreases with the larger effective carrier mass.<sup>60,61</sup> We attribute the allowed Raman scattering of the coupled modes mainly to DP, because of their phononlike character.

### D. LOPC mode in the depletion layer

In our two-color experiments on  $n$ -GaAs (see Sec. IV D), we observe the LOPC mode whose frequency lies between  $\Omega_{LO}$  and  $\Omega_{TO}$ . The LOPC frequency cannot be reproduced by the usual undamped solutions of Eq. (9), indicating that it cannot be an LO-electron plasma-coupled mode. Instead, the frequency is close to that of the LO-hole plasma coupled mode.

Raman studies on  $p$ -doped GaAs found that the LO-hole coupled mode frequency decreases from the  $\Omega_{LO}$  to the  $\Omega_{TO}$  limit with increasing hole density in the range of  $n_{\text{dope}} = 5 \times 10^{18} - 2 \times 10^{19} \text{ cm}^{-3}$ .<sup>22–24,59,62</sup> Equation (7) reproduced well the carrier-density-dependent frequency by assuming a large plasmon damping,  $\gamma > 9 \text{ THz}$ .<sup>22–24</sup> At hole densities below  $2 \times 10^{18} \text{ cm}^{-3}$ , the LO-hole coupled mode was not observed as a distinct mode either in Raman scattering<sup>22,23</sup> or as a coherent oscillation in transient reflectivity,<sup>8,9</sup> because its frequency is very close to  $\Omega_{LO}$ .

The coherent LO-hole coupled mode can appear even in  $n$ -GaAs under the appropriate circumstances. It was reported in a surface-sensitive TR-SHG study on  $n$ -GaAs and was attributed to the LO-phonon coupled with photoinjected hole plasma in the depletion layer.<sup>50</sup> Coherent LO-electron coupled mode in the depletion layer was also observed in the same experiment. The LO-hole and LO-electron couplings are expected to dominate at the top surface and in the deeper depletion layer, respectively, because holes and electrons are swept by the built-in depletion field toward the surface and into the bulk. The frequencies of the LO-hole and LO-electron coupled modes in the TR-SHG study were reproduced over a wide range of photoexcited plasma densities by Eq. (7) assuming  $\Gamma = 0.25 \text{ THz}$  for the LO phonon,  $\gamma_e = 0.1 \text{ THz}$  for electrons, and  $\gamma_h = 25 \text{ THz}$  for holes.<sup>50</sup>

Because our reflectivity measurement with 3.1 eV light is also sensitive to the surface dynamics [see Fig. 2], we can likewise assign the coherent modes at  $\sim 8.2$  and  $6.7 \text{ THz}$  [see Figs. 9–11] to the LO-hole and LO-electron coupled modes in different regions of the depletion layer. The carrier density

dependence of the LO-hole dephasing rate and frequency [see Figs. 10(b) and 10(c)] is in qualitative agreement with that of the TR-SHG study.<sup>50</sup> There is a significant discrepancy in the photoexcited carrier density (averaged over the photoexcited volume), however; our LO-hole frequency downshifts to 8.2 THz and dephasing increases to 2.5 ps<sup>-1</sup> already at  $2.5 \times 10^{17}$  cm<sup>-3</sup>, whereas those in the TR-SHG study did so at  $1.4 \times 10^{19}$  cm<sup>-3</sup>. Also, our LO-electron mode appears much weaker than the LO-hole counterpart [see Fig. 11(a)], whereas in the TR-SHG study the two FT peaks were comparable in height. These differences suggest that the linear detection with the 3.1 eV probe is more sensitive to the top surface layer, at which the effective hole density is largest because of the ultrafast drift diffusion, than the SHG detection with 1.55 eV light. Indeed, the probing depth in the SHG experiment on GaAs, which is noncentrosymmetric and therefore has a bulk contribution, is given by the penetration depth of 3.1 eV SHG light, because the SHG light traverses the probing region only once, rather than one half of the penetration depth in the reflectivity detection. The positive chirp of our LO-hole mode [see Fig. 10(d)], which is indicative of a decreasing carrier density, can be explained by diffusion of holes into the bulk on the picosecond time scale.

### E. Anisotropy in frequencies and dephasing rates of LO and LOPC modes

A novel feature of the present study is the dependence of the frequency and dephasing rate of the LO and LOPC modes of *n*-GaAs on the probe polarization angle  $\theta$  [see Fig. 8]. Such behavior is not observed for the LO phonon of *i*-GaAs and the optical phonon of Ge, under the same experimental conditions. We therefore explain the  $\theta$  dependence for *n*-GaAs by assuming small differences in the frequency and the dephasing rates between the anisotropic dipole-allowed and isotropic dipole-forbidden components.

We express the reflectivity modulation due to the LO phonon  $\Delta R_{LO}$  as a superposition of the two damped oscillators:

$$\begin{aligned} \Delta R_{LO}(\theta, t) = & C_{LO} \exp(-\Gamma_{LOF}t) \sin(2\pi \Omega_{LOF}t + \psi_{LOF}) \\ & + D_{LO} \cos(2\theta) \exp(-\Gamma_{LOA}t) \\ & \times \sin(2\pi \Omega_{LOA}t + \psi_{LOA}), \end{aligned} \quad (13)$$

where the subscripts LOF and LOA, respectively, stand for the forbidden and allowed Raman processes. We can reasonably reproduce the  $\theta$ -dependent LO amplitude, dephasing rate, and frequency by assuming  $D_{LO}/C_{LO} = 6.5$ ,  $\Gamma_{LOF} = 0.65$  ps<sup>-1</sup>,  $\Gamma_{LOA} = 0.41$  ps<sup>-1</sup>,  $\Omega_{LOF} = 8.64$  THz,  $\Omega_{LOA} = 8.69$  THz, and  $\psi_{LOF} = \psi_{LOA}$ , as indicated with solid curves in Figs. 8(a) and 8(c). Both quantities diverge near  $\theta \sim \pm 45^\circ$  where the amplitude of the superposed oscillation vanishes.

There is no intrinsic mechanism to cause anisotropy in the  $q = 0$  LO phonon frequency and dephasing rate in a perfect cubic crystal. However, a similar but larger splitting between the allowed and forbidden Raman scatterings was reported for the LO phonon frequency of an Al<sub>x</sub>Ga<sub>1-x</sub>As crystal<sup>63,64</sup> and of an ion-etched InP,<sup>65</sup> and attributed to contribution from scattering by  $q \neq 0$  phonons in the presence of structural disorder. Also, anisotropy in plasma and phonon damping was reported for semi-insulating and

*n*-type GaAs, and attributed to anisotropic strain induced by point defects (dopants) and dislocations in the near-surface region.<sup>66</sup> We therefore attribute the observed anisotropy in the LO frequency and dephasing rate to large  $q$  phonons ( $\sim 0.2/a_0$ <sup>34</sup>) involved in the impurity-induced  $F_i$  scattering. The range of  $q$  contributing to the  $F_i$  scattering could lead to a maximum downshift of the LO frequency by  $\lesssim 0.1$  THz, according to the phonon dispersion relation,<sup>67</sup> which is in reasonable agreement with our analysis ( $\Omega_{LOF} - \Omega_{LOA} = -0.05$  THz). The faster dephasing for the isotropic forbidden component can be explained by the distribution of frequencies of phonons with different  $q$ .

The  $\theta$ -dependent  $L-$  frequency and dephasing rate [see Figs. 8(b) and 8(d)] can be explained in the similar way. The experimental data are reasonably reproduced for  $D_{L-}/C_{L-} = -0.2$ ,  $\Gamma_{L-F} = 2.21$  ps<sup>-1</sup>,  $\Gamma_{L-A} = 1.8$  ps<sup>-1</sup>,  $\Omega_{L-F} = 7.515$  THz,  $\Omega_{L-A} = 7.43$  THz, and  $\psi_{L-F} = \psi_{L-A}$ , with the subscripts  $L-F$  and  $L-A$  denoting the forbidden and allowed  $L-$  scattering processes replacing LOF and LOA in Eq. (13). No divergence occurs at  $\theta = \pm 45^\circ$  for the  $L-$  mode, because the amplitude of the forbidden contribution is larger than the allowed contribution, and therefore the superposed oscillation never vanishes.

For the  $L-$  mode, the origin of the splitting cannot be attributed to  $F_i$  scattering, because the impurity potential is screened in the heavily doped bulk. The time-dependent surface field, which was proposed in Ref. 16, cannot be the origin either, because the FK effect is negligible for the bulk LOPC mode. According to the electronic Raman scattering theory based on the Lindhard dielectric function, the Raman line shape (frequency and linewidth) detected in the allowed and forbidden geometries can be different, because the former is determined by the interference between the DP and EO scatterings, and the latter by the interference between the CDF and F scatterings.<sup>31,32,58</sup> The peak shift direction in our study is opposite from the theoretical prediction<sup>31,32</sup> and the experimental observation,<sup>58</sup> however. We therefore tentatively attribute the splitting to the contribution of the large  $q$  phonons due to the  $q^2$  dependence of the CDF mechanism in the isotropic component. The higher  $L-$  frequency for the forbidden scattering than for the allowed scattering is consistent with the dispersion relation of the coupled mode in which the frequency upshifts with increasing  $q$ .<sup>57,58</sup>

## VI. CONCLUSION

We have investigated the detection mechanisms of the coherent LO and LOPC modes of GaAs in transient reflectivity measurements at the  $E_0$  and  $E_1$  gaps. The probe polarization angle dependence of the coherent amplitudes can be explained in terms of a coherent superposition of the dipole-allowed and dipole-forbidden Raman scatterings involved in the modulation of reflectivity by the lattice and electronic polarizations. This also leads to the probe-polarization dependent frequencies and dephasing rates arising from different  $q$  dependence of the allowed and forbidden mechanisms. With near ultraviolet light probing at the  $E_1$  gap, the transient reflectivity detection can monitor exclusively the surface depletion layer in which the coherent response is dominated by unscreened LO phonons as well as LO phonons coupled with the photoexcited and

spatially separated hole and electron plasmas. The observed coherent response demonstrates strong interaction between the lattice and spatiotemporal charge carrier dynamics under inhomogeneous carrier generation and subpicosecond time scale nondiffusive transport.

## ACKNOWLEDGMENTS

The authors would like to thank K. Benedix for editing the manuscript. H.P. is grateful to NSF grant CHE-0650756 for financial support.

\*ishioka.kunie@nims.go.jp

- <sup>1</sup>T. Dekorsy, G. C. Cho, and H. Kurz, in *Light Scattering in Solids VIII*, edited by M. Cardona and G. Güntherodt (Springer, Berlin, 2000), p. 169.
- <sup>2</sup>M. Först and T. Dekorsy, in *Coherent Vibrational Dynamics*, edited by S. D. Silvestri, G. Cerullo, and G. Lanzani (CRC, Boca Raton, 2007), p. 129.
- <sup>3</sup>K. Ishioka and O. V. Misochko, in *Progress in Ultrafast Intense Laser Science V*, edited by K. Yamanouchi, A. Giullietti, and K. Ledingham (Springer, Berlin, 2010), p. 23.
- <sup>4</sup>L. Dhar, J. Rogers, and K. A. Nelson, *Chem. Rev.* **94**, 157 (1994).
- <sup>5</sup>T. E. Stevens, J. Kuhl, and R. Merlin, *Phys. Rev. B* **65**, 144304 (2002).
- <sup>6</sup>H. J. Zeiger, J. Vidal, T. K. Cheng, E. P. Ippen, G. Dresselhaus, and M. S. Dresselhaus, *Phys. Rev. B* **45**, 768 (1992).
- <sup>7</sup>G. C. Cho, W. Kütt, and H. Kurz, *Phys. Rev. Lett.* **65**, 764 (1990).
- <sup>8</sup>T. Pfeifer, T. Dekorsy, W. Kutt, and H. Kurz, *Appl. Phys. A* **55**, 482 (1992).
- <sup>9</sup>T. Dekorsy, T. Pfeifer, W. Kütt, and H. Kurz, *Phys. Rev. B* **47**, 3842 (1993).
- <sup>10</sup>M. Hase, K. Mizoguchi, H. Harima, S. I. Nakashima, and K. Sakai, *Phys. Rev. B* **58**, 5448 (1998).
- <sup>11</sup>K. Ishioka, M. Hase, M. Kitajima, and K. Ushida, *Appl. Phys. Lett.* **78**, 3965 (2001).
- <sup>12</sup>K. Ishioka, M. Hase, K. Ushida, and M. Kitajima, *Physica B* **316-317**, 296 (2002).
- <sup>13</sup>K. Ishioka, M. Hase, M. Kitajima, L. Wirtz, A. Rubio, and H. Petek, *Phys. Rev. B* **77**, 121402 (2008).
- <sup>14</sup>O. V. Misochko, K. Ishioka, M. Hase, and M. Kitajima, *J. Phys. Condens. Matter* **19**, 156227 (2007).
- <sup>15</sup>A. Kim, J. Callan, C. Roeser, and E. Mazur, *Phys. Rev. B* **66**, 245203 (2002).
- <sup>16</sup>G. C. Cho, H. J. Bakker, T. Dekorsy, and H. Kurz, *Phys. Rev. B* **53**, 6904 (1996).
- <sup>17</sup>T. Pfeifer, W. Kütt, H. Kurz, and R. Scholz, *Phys. Rev. Lett.* **69**, 3248 (1992).
- <sup>18</sup>R. Scholz, T. Pfeifer, and H. Kurz, *Phys. Rev. B* **47**, 16229 (1993).
- <sup>19</sup>P. Y. Yu and M. Cardona, *Fundamentals of Semiconductors* (Springer, Berlin, 2001).
- <sup>20</sup>K. J. Yee, Y. S. Lim, T. Dekorsy, and D. S. Kim, *Phys. Rev. Lett.* **86**, 1630 (2001).
- <sup>21</sup>A. Mooradian and A. L. McWhorter, *Phys. Rev. Lett.* **19**, 849 (1967).
- <sup>22</sup>R. Fukasawa and S. Perkowitz, *Phys. Rev. B* **50**, 14119 (1994).
- <sup>23</sup>R. Fukasawa and S. Perkowitz, *Jpn. J. Appl. Phys.* **35**, 132 (1996).
- <sup>24</sup>G. Irmer, M. Wenzel, and J. Monecke, *Phys. Rev. B* **56**, 9524 (1997).
- <sup>25</sup>V. Vorliceck, I. Gregora, W. Kauschke, J. Menendez, and M. Cardona, *Phys. Rev. B* **42**, 5802 (1990).
- <sup>26</sup>W. Kauschke, N. Mestres, and M. Cardona, *Phys. Rev. B* **36**, 7469 (1987).
- <sup>27</sup>R. Huber, F. Tausser, A. Brodschelm, M. Bichler, G. Abstreiter, and A. Leitenstorfer, *Nature (London)* **414**, 286 (2001).
- <sup>28</sup>R. Huber, C. Kübler, S. Tübel, A. Leitenstorfer, Q. T. Vu, H. Huang, F. Köhler, and M.-C. Amann, *Phys. Rev. Lett.* **94**, 027401 (2005).
- <sup>29</sup>G. C. Cho, T. Dekorsy, H. J. Bakker, R. Hövel, and H. Kurz, *Phys. Rev. Lett.* **77**, 4062 (1996).
- <sup>30</sup>M. Hase, S. Nakashima, K. Mizoguchi, H. Harima, and K. Sakai, *Phys. Rev. B* **60**, 16526 (1999).
- <sup>31</sup>M. V. Klein, in *Light Scattering in Solids I*, edited by M. Cardona (Springer, Berlin, 1983), p. 147.
- <sup>32</sup>M. V. Klein, B. N. Ganguly, and P. J. Colwell, *Phys. Rev. B* **6**, 2380 (1972).
- <sup>33</sup>A. K. Sood, W. Kauschke, J. Menendez, and M. Cardona, *Phys. Rev. B* **35**, 2886 (1987).
- <sup>34</sup>J. Menéndez and M. Cardona, *Phys. Rev. B* **31**, 3696 (1985).
- <sup>35</sup>W. Kauschke, M. Cardona, and E. Bauser, *Phys. Rev. B* **35**, 8030 (1987).
- <sup>36</sup>A. Pinczuk, G. Abstreiter, R. Trommer, and M. Cardona, *Solid State Commun.* **30**, 429 (1979).
- <sup>37</sup>C. Y. Chen, *Phys. Rev. B* **27**, 1436 (1983).
- <sup>38</sup>W. Kauschke and M. Cardona, *Phys. Rev. B* **33**, 5473 (1986).
- <sup>39</sup>S. M. Sze, *Semiconductor Devices, Physics and Technology*, 2nd ed. (Wiley, New York, 2002), p. 176.
- <sup>40</sup>J. R. Chelikowsky and M. L. Cohen, *Phys. Rev. B* **14**, 556 (1976).
- <sup>41</sup>P. Lautenschlager, M. Garriga, S. Logothetidis, and M. Cardona, *Phys. Rev. B* **35**, 9174 (1987).
- <sup>42</sup>A. Othonos, *J. Appl. Phys.* **83**, 1789 (1998).
- <sup>43</sup>E. D. Palik, in *Handbook of Optical Constants of Solids*, edited by E. Palik (Academic Press, San Diego, 1985), p. 429.
- <sup>44</sup>We remove the reflectivity response for the first 250 fs after photoexcitation from our FT analysis because the nonoscillatory electronic response is too complex to be well defined by a simple mathematical function. Consequently, the appearance of the FT spectrum, i.e., the LO mode as a dip upon the  $L^-$  peak, in Fig. 5(b) is determined by the phase relation of the LO and  $L^-$  modes at  $t \sim 250$  fs, where the analyzed amplitude is largest. Extrapolation to  $t = 0$  suggests that the two modes have similar initial phase ( $\psi \simeq \pi/2$ ).
- <sup>45</sup>The  $L^-$  oscillation of  $n$ -GaAs is not perfectly reproduced by Eq. (11); its frequency downshifts with delay time, and its amplitude decays faster than an exponential function of time. This may reflect the depth gradient in the doped carrier density in the depletion region as well as the ultrafast drift diffusion of carriers.
- <sup>46</sup>The discrepancy between the experimental and calculated frequencies can be attributed to factors such as the time-dependent photocarrier distribution (effective mass) and density, which we surmise to evolve on the picosecond time scales from Fig. 3(a), as well as coherent mode damping that is not included in Eq. (9).
- <sup>47</sup>Y.-M. Chang, *Appl. Phys. Lett.* **82**, 1781 (2003).

- <sup>48</sup>The slow ( $\sim 1$  THz) modulation seen in Fig. 9(a) is unexpected for GaAs and may be an artifact of the laser amplitude instability.
- <sup>49</sup>H. W. K. Tom, Y. M. Chang, and H. Kwak, *Appl. Phys. B* **68**, 305 (1999).
- <sup>50</sup>Y.-M. Chang, *Appl. Phys. Lett.* **80**, 2487 (2002).
- <sup>51</sup>W. Mönch, *Semiconductor Surfaces and Interfaces* (Springer, Berlin, 2001), p. 167.
- <sup>52</sup>K. Kato, K. Ishioka, M. Kitajima, J. Tang, R. Saito, and H. Petek, *Nano Lett.* **8**, 3102 (2008).
- <sup>53</sup>I. Katayama, S. Koga, K. i. Shudo, J. Takeda, T. Shimada, A. Kubo, S. Hishita, D. Fujita, and M. Kitajima, *Nano Lett.* **11**, 2648 (2011).
- <sup>54</sup>R. Trommer and M. Cardona, *Phys. Rev. B* **17**, 1865 (1978).
- <sup>55</sup>A. Pinczuk and E. Burstein, *Phys. Rev. Lett.* **21**, 1073 (1968).
- <sup>56</sup>A. Pinczuk and E. Burstein, *Surf. Sci.* **37**, 153 (1973).
- <sup>57</sup>A. Pinczuk, G. Abstreiter, R. Trommer, and M. Cardona, *Solid State Commun.* **21**, 959 (1977).
- <sup>58</sup>G. Abstreiter, R. Trommer, M. Cardona, and A. Pinczuk, *Solid State Commun.* **30**, 703 (1979).
- <sup>59</sup>D. Olego and M. Cardona, *Phys. Rev. B* **24**, 7217 (1981).
- <sup>60</sup>M. Sakai, H. Shibata, and M. Shinohara, *J. Phys. Soc. Jpn.* **70**, 1064 (2001).
- <sup>61</sup>J. P. Estrera, W. M. Duncan, and R. Glosser, *Phys. Rev. B* **49**, 7281 (1994).
- <sup>62</sup>K. Wan and J. F. Young, *Phys. Rev. B* **41**, 10772 (1990).
- <sup>63</sup>I. Sela, V. V. Gridin, R. Beserman, R. Sarfaty, D. Fekete, and H. Morkoc, *J. Appl. Phys.* **63**, 966 (1988).
- <sup>64</sup>M. E. Delaney, T. C. McGlenn, M. V. Klein, and H. Morkoc, *Phys. Rev. B* **44**, 8605 (1991).
- <sup>65</sup>J. E. Maslar, S. R. Kisting, P. W. Bohn, I. Adesida, D. G. Ballegeer, C. Caneau, and R. Bhat, *Phys. Rev. B* **46**, 1820 (1992).
- <sup>66</sup>Yu. A. Kosevich, J. Ortega-Gallegos, A. G. Rodriguez, L. F. Lastras-Martinez, and A. Lastras-Martinez, *Phys. Status Solidi C* **0**, 2982 (2003).
- <sup>67</sup>J. L. T. Waugh and G. Dolling, *Phys. Rev.* **132**, 2410 (1963).